

Deep graph kernel point processes

Zheng Dong¹, Matthew Repasky¹, Xiuyuan Cheng², and Yao Xie^{*1}

¹ H. Milton Stewart School of Industrial & Systems Engineering, Georgia Institute of Technology

² Department of Mathematics, Duke University

Abstract

Point process models are widely used to analyze asynchronous events occurring within a graph that reflect how different types of events influence one another. Predicting future events' times and types is a crucial task, and the size and topology of the graph add to the challenge of the problem. Recent neural point process models unveil the possibility of capturing intricate inter-event-category dependencies. However, such methods utilize an unfiltered history of events, including all event categories in the intensity computation for each target event type. In this work, we propose a graph point process method where event interactions occur based on a latent graph topology. The corresponding undirected graph has nodes representing event categories and edges indicating potential contribution relationships. We then develop a novel deep graph kernel to characterize the triggering and inhibiting effects between events. The intrinsic influence structures are incorporated via the graph neural network (GNN) model used to represent the learnable kernel. The computational efficiency of the GNN approach allows our model to scale to large graphs. Comprehensive experiments on synthetic and real-world data show the superior performance of our approach against the state-of-the-art methods in predicting future events and uncovering the relational structure among data.

Keywords: Point Processes with Graph, Non-Stationary Influence Kernel, Graph Neural Networks

1 Introduction

Point processes represent a prominent category of stochastic models designed to capture discrete events occurring over time. Modern applications are often characterized by the presence of separate categories of events, known as *marks*, which encapsulate attributes such as specific locations or types of events. The occurrence of one type of event can influence the occurrence of future events of the same or another type, and the identification of dependencies among events plays a crucial role in predicting and understanding upcoming asynchronous events. For example, crime linkage analysis [46] provides insight for criminal pattern detection and decision-making to practitioners. Historical interactions between users and groups on social networks favor accurate future recommendations aligned with their individual interests. When these influence structures can be represented by a *graph*, such models can be referred to as graph point processes.

*Email: yao.xie@isye.gatech.edu

There exists a wide range of methods for modeling graph point processes. Classical multivariate Hawkes processes [29] assume a parametric form of the conditional intensity. Many modern approaches focus on modeling a more general form of the intensity of events incorporated with the graph structure, adopting function approximators such as neural networks. For example, recent approaches utilize self-attention with respect to the latent graph structure to reflect inter-node influence on the graph [40, 47]. However, such approaches often assume some parametric restriction on the form of the conditional intensity, potentially leading to degraded performance and hindering interpretability. Furthermore, these methods only model single-hop influence on the latent graph based on the adjacency matrix.

Graph neural networks (GNNs) have been a rapidly developing tool for extracting informative patterns from graph-structured data [37]. For instance, message passing GNNs have been widely used in the context of point processes for relationship inference [43], temporal interaction prediction [38], and event propagation modeling [36]. A specific approach would be convolutional GNNs, which generalize the operation of convolution in neural networks from grid data to graph data. They allow models to capture cyclic mutual dependencies of graph nodes and are efficient enough to be scaled to large graphs. Convolutional GNNs can thereby provide a framework for flexible modeling of point processes on graphs, yielding superior prediction performance and interpretability.

Contribution: In this paper, we propose a novel framework for modeling general influence kernels in point processes on latent graphs based on GNNs, which inform potential event category relationships and provide reliable predictions for future events. Specifically, the kernel integrates a unified framework for convolutional GNNs based on localized graph filter basis functions, and is flexible enough to capture non-stationary inter-node event promotion, inhibition, and multi-hop effects. Our model with the proposed influence kernel provides an efficient, effective, and interpretable object for point process modeling on large graphs.

The contributions in this paper can be summarized as follows:

1. Our proposed method explicitly models the influence kernel in point processes via convolutional GNNs as opposed to typical intensity-based models. This permits greater expressivity of inter-event-category contributions, including non-stationary, multi-hop exciting, and inhibiting effects. Furthermore, the graph kernel can be directly interpreted, yielding clear information about the relational structure in the modeled graph point process.
2. The proposed convolutional-GNN-based deep kernel can be efficiently scaled to large graphs by taking advantage of the localized graph filter basis. The basis allows the deep kernel to go beyond simple distance-based influence for graphs representing events in space, providing a model structure for non-spatial graphs such as social networks. Meanwhile, a larger class of GNN models can be incorporated within our framework, enabling broader versatility in real-world applications.
3. Comprehensive experiments demonstrate that including the latent graph structure in the deep kernel modeling yields benefits over the states-of-the-art in both simulated and real data settings. Our method is applicable to a wide array of point process data settings, including events generated by infrastructural, climatic, and social phenomena.

1.1 Related Works

Using machine learning to model influence between different event types is a long-studied area in the point process literature. Seminal point process works construct parametric models of the conditional intensity [15, 25], which are often not expressive enough to capture complex influence mechanisms. Common approaches to achieve more expressive conditional intensity models [13, 22] utilize recurrent neural networks (RNNs). Due to advances in attention models for sequential data modeling [34], RNN approaches have been surpassed by self-attention approaches, which include the Transformer Hawkes Process (THP) [47] and the Self-Attentive Hawkes Process (SAHP) [40]. These RNN and self-attention methods provide expressive models for the conditional intensity, however they often suffer from high computational cost and lack of model interpretability. Instead of modeling the conditional intensity, many recent approaches recover the influence kernel in point processes [12, 26, 45]. Learned influence kernels provide a direct means for interpreting inter-event influence in point processes; however, prior works have not exploited graph structure in kernel models, while we incorporate graph topology in the construction of the influence kernel. Alternative approaches have been proposed [27, 31] for flexible modeling of the conditional probability or cumulative probability function. Nonetheless, they decouple the distributions of event time and type and the model expressiveness is still limited.

In contemporary applications, the collection of point process data often reveals an underlying latent graph structure, leading to the widespread adoption of models incorporating graph structures for a variety of purposes. A common goal is to infer the topology of the latent graph existing in asynchronous discrete event data, such as for individual event dependence modeling [20] or for relation inference between event types in [2, 6, 43]. Our proposed model aims for learning point processes with influence kernels and has the capability to recover the kernel (graph) structure, discover event dependency, and predict events simultaneously. The Geometric Hawkes Process (GHM) [30] combines the Hawkes process with graph convolution RNNs, exploiting graph structure in order to learn marked Hawkes processes and predict future events. However, this approach still assumes a parametric form for the conditional intensity function. Recent studies adopt attention-based mechanisms for point process modeling and lend themselves naturally to a graphical interpretation of the event influence structure. The learned attention weights in the Attentive Neural Hawkes Process (A-NHP) [39] can be interpreted to represent the underlying graph structure. Another study [41] extends SAHP to events on a learned latent graph, and event influences are modeled according to the edges of the graph. However, these approaches consider only single-hop, adjacency-based influence on the latent graph. In our work, the incorporation of localized graph filters in graph convolution permits the recovery of complex event dependency, such as multi-hop influence mechanisms, according to the graph topology, and holds the potential to integrate either spatial- or spectral-based graph neural network structures.

Our work is related to GNNs, which have seen wide applications to areas including temporal phenomena on graphs [21, 37]. The popularity of graph convolutions in GNNs has been rapidly growing in recent years. They incorporate spatial convolutions considering propagation according to the adjacency structure in the graph or spectral convolutions based upon the graph Laplacian [5]. An early attempt applying spatial convolutions is the Diffusion-convolutional neural networks (DCNN) [1] by graph diffusion processes. Other spatial-based approaches include attention models such as the Graph Attention Network (GAT) [4, 35] and the Graph Transformer [14]. Prototypical

spectral convolutions based on Chebyshev polynomials of the graph Laplacian are utilized in Chebnet [10] and graph convolutional networks (GCN) [19], with recent extensions including auto-regressive moving average (ARMA) spectral convolutions [3] and the Simple Spectral Graph Convolution (SSGC) constructed via a Markov diffusion kernel [44]. Modern approaches incorporate both local and global features, such as the flexible combination of spatial and spectral convolutions in L3Net [8] and of local filters and global attention in the General, Powerful, Scalable (GPS) Graph Transformer [28]. Practically, GNN models can often be applied to model event occurrences on graphs, such as anomaly detection using GCNs [7], graph attention [11], and combined spatial/spectral techniques [33] and change point detection using transformer convolutions [42] and GATs [32].

2 Background

Temporal point process (TPP). A TPP [29] models the occurrence of discrete events that depend on the observed history in a continuous time domain. Let $\mathcal{H} = \{t_1, \dots, t_n\}$ be an observed event sequence, where $t_i \in [0, T] \subset \mathbb{R}$ is the time of i -th event. We denote the history before a given time t as $\mathcal{H}_t = \{t_i | t_i < t\}$. The conditional intensity of events is defined as $\lambda(t) = \lim_{\Delta t \downarrow 0} \mathbb{E}[\mathbb{N}([t, t + \Delta t]) | \mathcal{H}_t] / \Delta t$, where the counting measure \mathbb{N} is defined as the number of events occurring in $[t, t + \Delta t]$. For notational simplicity, we omit the dependency of history \mathcal{H}_t in $\lambda(t)$. The well-known Hawkes process [15] models the self-excitation effect from history in an additive manner. The conditional intensity function is defined as

$$\lambda(t) = \mu + \sum_{t' \in \mathcal{H}_t} k(t', t),$$

where μ is the background intensity, and k is the so-called influence kernel measuring the effects of historical events.

In a *marked point process*, each event is associated with an additional attribute called *mark* denoted by $v \in V$. The mark represents specific characteristics of the event and can be either continuous or categorical, such as event location or event type. Let $\mathcal{H} = \{(t_i, v_i)\}_{i=1}^n$ and $\mathcal{H}_t = \{(t_i, v_i) | t_i < t\}$ be the observed event sequence and history before time t , respectively. The conditional intensity with influence kernel k can be written as:

$$\lambda(t, v) = \mu + \sum_{(t', v') \in \mathcal{H}_t} k(t', t, v', v). \quad (1)$$

The influence kernel is crucial when learning the conditional intensity $\lambda(t, v)$ from event sequences. Our kernel goes beyond the parametric kernel in the classic Hawkes process and leverages latent data structures, enabling us to better capture the underlying event generating mechanism.

Graph convolution. Graph convolutions in graph neural networks [37] extend the convolution strategy to the graph and address the problem of cyclic mutual dependencies architecturally. Graph convolutions fall into two categories: spectral- and spatial-based models. Spectral graph convolutions introduce graph filters g_θ based on the full eigen-decomposition of the graph Laplacian. The graph signal X is convoluted by $X *_G g_\theta = U g_\theta U^T X$, where U is the matrix of the eigenvectors

of the graph Laplacian ordered by eigenvalues. For instance, in Spectral Convolutional GNNs [5], the graph filter $g_\theta = \Theta_{i,j}$ contains a set of learnable parameters that characterize the relations between node pairs. On the other hand, spatial-based graph convolution is performed by information propagation along edges. The weight matrix in each layer is constructed based on the node’s spatial relations (*i.e.*, adjacency matrix). Either the localized filter or the weight matrix plays a pivotal role in capturing the nodal dependencies. Various structures of graph convolutions, both spectral and spatial, can be integrated into our proposed influence kernel to describe a wide spectrum of intricate inter-event-category dependencies.

3 Point processes on graphs

3.1 Problem definition

The objective of this study is to construct a point process model for the occurrence of multiple types of events within a latent graph structure. Let $G = (V, E)$ denote the underlying graph, where each node $v \in V$ represents one event type. An undirected edge connecting nodes u and v indicates the existence of potential interaction between type- u and type- v events. Note that the edges merely suggest the support of possible inter-event-category interactions without dictating the directions.

Consider a set of event sequences $\mathcal{S} = \{\mathcal{H}^1, \mathcal{H}^2, \dots, \mathcal{H}^{|\mathcal{S}|}\}$, where each $\mathcal{H}^s = \{(t_i^s, v_i^s)\}_{i=1}^{n_s}$ is a collection of events (t_i^s, v_i^s) occurring on node v_i^s at time t_i^s . Our proposed graph point process is expected to: (i) jointly predict the times and types of forthcoming events based on the observed historical data and (ii) provide an interpretable understanding of the event generation process by revealing the interdependences among multiple types of events. Toward this end, we adopt the statistical formulation of conditional intensity in (1) and introduce an influence kernel built on convolutional GNN components, aiming to explicitly characterize the complicated contributing relationship between any binary event pair (*e.g.*, excitation, inhibition, or other dynamic influences).

3.2 Deep temporal graph kernel

Modeling the multi-dimensional influence kernel k for intricate event dependency is crucial yet challenging. To go beyond simple parametric forms of the kernel while maintaining the model efficiency, we represent the multi-dimensional kernel by taking advantage of the kernel singular value decomposition (SVD) [23, 24]. Specifically, the influence kernel $k(t', t, v', v)$ in (2) is decomposed into basis kernel functions as follows:

$$k(t', t, v', v) = \sum_{d=1}^D \sigma_d g_d(t', t - t') h_d(v', v), \quad (2)$$

where $\{g_d, h_d\}_{d=1}^D$ are sets of basis kernels in terms of event time and type, respectively. The scalar σ_d is the corresponding weight (or “singular value”) at each rank d . Instead of directly learning the multi-dimensional event dependency, we simplify the task by “separately” modeling specific modes of event dependency over time or graph using different basis kernels. It is worth noting that the weighted combination of basis kernels covers a broad range of non-stationary influence kernels used in point processes, and our kernel k is not decoupled over time and graph space. While functional

SVD is usually infinite-dimensional, in practice, we can truncate the decomposition as long as the singular values σ_k decay sufficiently fast, only considering a finite rank representation.

The temporal basis kernels are carefully designed to capture the heterogeneous temporal dependencies between past and future events. First, the parametrization of temporal kernels $\{g_d\}_{d=1}^D$ using displacements $t - t'$ instead of t provides us a low-rank way to approximate general kernels [12]. To proceed, we approximate $\{g_d\}_{d=1}^D$ using shared basis functions:

$$g_d(t', t - t') = \sum_{l=1}^L \beta_{dl} \psi_l(t') \varphi_l(t - t'), \quad \forall d = 1, \dots, D.$$

Here $\{\psi_l, \varphi_l : [0, T] \rightarrow \mathbb{R}\}_{l=1}^L$ are two sets of one-dimensional basis functions characterizing the temporal impact of an event occurring at t' and the decaying pattern of that impact spread over $t - t'$. The scalar β_{dl} is the corresponding weight. Each of the basis functions $\{\psi_l, \varphi_l\}_{l=1}^L$ are represented by a fully-connected neural network. The universal approximation power of neural networks enables the model to go beyond specific parametric forms of the influence kernel or conditional intensity.

3.3 Graph kernel with localized graph filters

We develop a novel framework for the graph basis kernels by leveraging the localized graph filters in graph convolution to extract informative inter-event-category patterns from graph-structured data. Specifically, the basis kernels $\{h_d\}_{d=1}^D$ are represented as follows:

$$h_d(v', v) = \sum_{r=1}^R \gamma_{dr} B_r(v', v), \quad \forall d = 1, \dots, D,$$

where $\{B_r(v', v) : V \times V \rightarrow \mathbb{R}\}_{r=1}^R$ are R bases of localized graph filters, and γ_{dr} is the corresponding weight for each B_r . The bases can be constructed either from a spatial or a spectral approach, corresponding to two categories of commonly-seen graph convolutions.

To showcase the model flexibility of our graph basis kernel, we present four examples of incorporating various localized graph filters in spectral- or spatial-based GNNs into our proposed frameworks. These include (Details are given in Appendix A):

- (1) *Chebnet* [10]: we let $B_r = T_{r-1}(\tilde{L})$, where T_r is the Chebyshev polynomial of order r evaluated at the scaled and normalized graph Laplacian $\tilde{L} = 2L/\lambda_{\max} - I$. Here $L = I - D^{-1/2}AD^{-1/2}$, D is the degree matrix, A is the adjacency matrix, and λ_{\max} is the largest eigenvalue of L .
- (2) *L3Net* [8]: we choose an integer o_r for each B_r , and $B_r(v', v) \neq 0$ only if $v \in N_{v'}^{(o_r)}$, where $N_{v'}^{(o_r)}$ denotes the set of o_r -th order neighbors of v' . Note that the neighborhood orders (o_1, \dots, o_R) can be adjusted accordingly with duplication, and all bases $\{B_r\}_{r=1}^R$ are trainable.
- (3) *GAT* [35] with R attention heads: each $B_r(v', v)$ is a learnable localized graph filter with positive entries and column-wise summation normalized to one (i.e., a learnable affinity matrix).
- (4) *GPS Graph Transformer* [14] with R attention and MPNN layers: we introduce $\{B_r(v', v)\}_{r=1}^{2R}$. For $\forall r \in \{1, \dots, R\}$, B_r is a learnable affinity matrix, and B_{2r} is the adjacency matrix A .

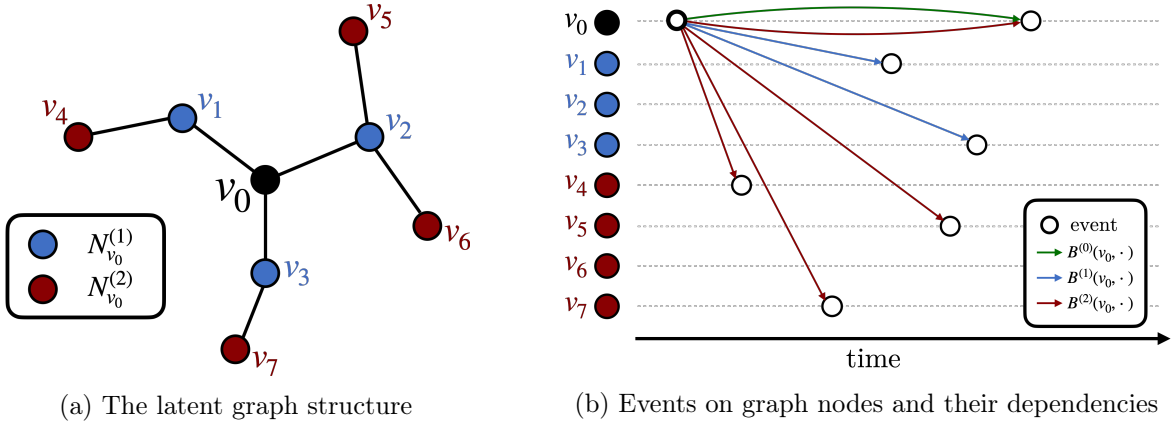


Figure 1: An example of modeling sequential events on an 8-node graph using graph filter bases in L3Net: (a) The latent graph structure. Blue and red nodes represent the 1st and 2nd order neighbors of v_0 , denoted by $N_{v_0}^{(1)}$ and $N_{v_0}^{(2)}$, respectively. (b) Three graph filter bases $B^{(0)}$, $B^{(1)}$, and $B^{(2)}$ capture the dependencies between events. Hollow circles are events observed on each node. Colored lines indicate the potential influence of the earliest type- v_0 event on future events captured by different bases.

By integrating the idea of localized graph filters in GNNs, the benefits of our design for the influence kernel k lie in the following concepts: (i) The kernel enables the adoption of various spectral and spatial filter bases. And the combination of R bases allows us to represent complex local and global patterns of inter-node influences with great model expressiveness. (ii) Our framework substantially reduces the number of model parameters to $\mathcal{O}(RC|V|)$ for modeling graph-structured point process data with $|V|$ event types, while classic multivariate point processes and other neural point processes typically require more than $\mathcal{O}(|V|^2)$ parameters. Here C represents the average local patch size [8]. In practice, we have $C, R \ll |V|$ when dealing with sparse graphs and considering only up to o -hop influence (commonly 2 or 3), which significantly improves the scalability of our model when applied to large graphs. Details of the complexity analysis can be found in Appendix A.

Formally, the temporal graph influence kernel k can be represented as:

$$k(t', t, v', v) = \sum_{r=1}^R \sum_{l=1}^L \alpha_{rl} \psi_l(t') \varphi_l(t - t') B_r(v', v), \quad (3)$$

where $\alpha_{rl} = \sum_{d=1}^D \sum_{r=1}^R \sum_{l=1}^L \sigma_d \beta_{dl} \gamma_{dr}$. For the experiments in this paper, we adopt the bases of localized graph filters in L3Net, for it provides a unified framework for both spatial- and spectral-based graph convolutions. Figure 1 illustrates the mechanism of the graph filter bases to capture the event dependencies during the modeling of sequential events on an 8-node graph. The neighborhood orders are highlighted as the superscripts of each graph filter basis.

3.4 Model estimation

To learn the model from data, we adopt the widely-used approach through MLE [29] by maximizing the log-likelihood of observing event sequences \mathcal{S} on $[0, T] \times V$:

$$\max_{\theta} \ell(\theta) := \frac{1}{|\mathcal{S}|} \sum_{s=1}^{|\mathcal{S}|} \left(\sum_{i=1}^{n_s} \log \lambda(t_i^s, v_i^s) - \sum_{v \in V} \int_0^T \lambda(t, v) dt \right). \quad (4)$$

Note that the model parameter θ is incorporated into the intensity function λ . Since negative values of the influence kernel are allowed for indicating inhibiting effects from past events, an additional constraint for the non-negativity of the conditional intensity function is required during model estimation. For this purpose, we use the log-barrier method for optimization in point processes [12], which maintains the model interpretability of the conditional intensity function with influence kernel while being computationally efficient. To be precise, we introduce an additional term $p(\theta, b)$ to the optimization problem that penalizes the value of intensity on a dense enough grid over space, denoted $\mathcal{U}_{\text{bar},t} \times V$ where $\mathcal{U}_{\text{bar},t} \subset [0, T]$. The final optimization problem is formulated as

$$\begin{aligned} \min_{\theta} \mathcal{L}(\theta) := & -\ell(\theta) + \frac{1}{w} p(\theta, b) = -\frac{1}{|\mathcal{S}|} \sum_{s=1}^{|\mathcal{S}|} \left(\sum_{i=1}^{n_s} \log \lambda(t_i^s, v_i^s) - \sum_{v \in V} \int_0^T \lambda(t, v) dt \right) \\ & - \frac{1}{w |\mathcal{S}| |\mathcal{U}_{\text{bar},t} \times V|} \sum_{s=1}^{|\mathcal{S}|} \sum_{t \in \mathcal{U}_{\text{bar},t}} \sum_{v \in V} \log(\lambda(t, v) - b), \end{aligned} \quad (5)$$

which is a combination of model log-likelihood and log-barrier penalization. Here, the scalar $w > 0$ is a weight to control the trade-off between log-likelihood and log-barrier, and $b > 0$ is a lower bound of the intensity value over space to guarantee the feasibility of logarithm. Both the weight w and lower bound b can be adjusted accordingly during optimization. Note that the optimization problem with log-barrier penalty can be computed efficiently. More details for model learning and computation are summarized in Appendix B and Appendix C Algorithm 1.

4 Experiment

In this section, we compare our method with deep graph kernel, referred to as **GrADK**, with five state-of-the-art point process methods on large-scale synthetic and real-world data sets. The superior performance of our model against baselines is demonstrated in terms of both recovering underlying event dependencies and predicting future events. More details and additional results are presented in Appendix D.

Baselines. Three of the baselines do not explicitly consider graph structure, including the (i) Recurrent Marked Temporal Point Process (RMTTP) [13], which uses a recurrent neural network to encode dependence through time; the (ii) Fully Neural Network model (FullyNN) [27], which models the cumulative distribution via a neural network; and the (iii) Deep Non-Stationary Kernel (DNSK) [12], which produces a low-rank neural-network-based influence kernel. We also include two baselines that encode graph information, including the (iv) Structured Transformer Hawkes

Process (THP-S) [47] and the (v) Graph Self-Attentive Hawkes Process (SAHP-G) [40] with a given graph structure, which both use self-attention mechanisms to represent the conditional intensity.

Experimental setup. We choose our one-dimensional temporal basis functions to be fully-connected neural networks with two hidden layers of width 32. Each layer is equipped with softplus activation function except the output layer. The bases of the localized graph filters take the form of the learnable bases in L3Net [8]. For each data set, all the models are trained using 80% of the data and tested on the remaining 20%. Our model parameters are estimated through (5) using the Adam optimizer [18] with a learning rate of 10^{-2} and batch size of 32. Details about the experimental setup for baselines can be found in Appendix D.

4.1 Synthetic data

We first evaluate the efficacy of our model on synthetic data. We generate three data sets using point processes with the following kernels and latent graph structures: (i) a non-stationary temporal kernel on a 3-node graph, (ii) a non-stationary temporal kernel on a 16-node graph with ring connectivity structure and 2-hop graph influence, and (iii) an exponentially decaying temporal kernel on a 50-node graph. Data sets are simulated using the thinning algorithm [9]. Each data set contains 1,000 sequences with an average length of 50.9, 105.8, and 386.8, respectively. Details regarding synthetic data are presented in Appendix D.

Kernel and intensity recovery. The first row of Figure 2 displays the true graph influence kernel in the 50-node synthetic data set and the learned graph kernels by GraDK, SAHP-G, and DNSK. Our method and DNSK directly learn the kernel, and the graph kernel in SAHP-G is constructed as in the original paper [40] by computing the empirical mean of the learned attention weights between nodes. While SAHP-G exaggerates the self-exciting influence of graph nodes and DNSK only learns some semblance of the graph kernel behavior, our method accurately recovers both self- and inter-node influence patterns, resulting in a faithful model of the true graph kernel. The conditional intensity via each method for one testing trajectory is displayed in the third row of Figure 2, which demonstrates the capability of our model to capture the temporal dynamics of events.

Similarly, Figure 3 contains the recovered graph kernel by each method for the synthetic data generated by the kernel on a 16-node ring graph with 2-hop influence. It is worth noting that our model learns an accurate representation, reconstructing the self-exciting and multi-hop influential structures in the ring graph, while SAHP-G only recovers the mutual dependencies within one-hop neighbors, restricted by their model formulation. The multi-hop influence along the graph structure is also reflected in the true and recovered event intensity by GraDK (the bottom row of Figure 3). The conditional intensities of SAHP-G and DNSK, however, either fail to capture the magnitude of this interdependence or do not accurately decay node dependence along the ring-structure connections.

Event dependency. Our model also exhibits exceptional performance in capturing sequential event dependencies. The second row of Figure 2 visualizes the learned inter-event dependency given a sample sequence from the testing set. The dependency between a prior and a future event

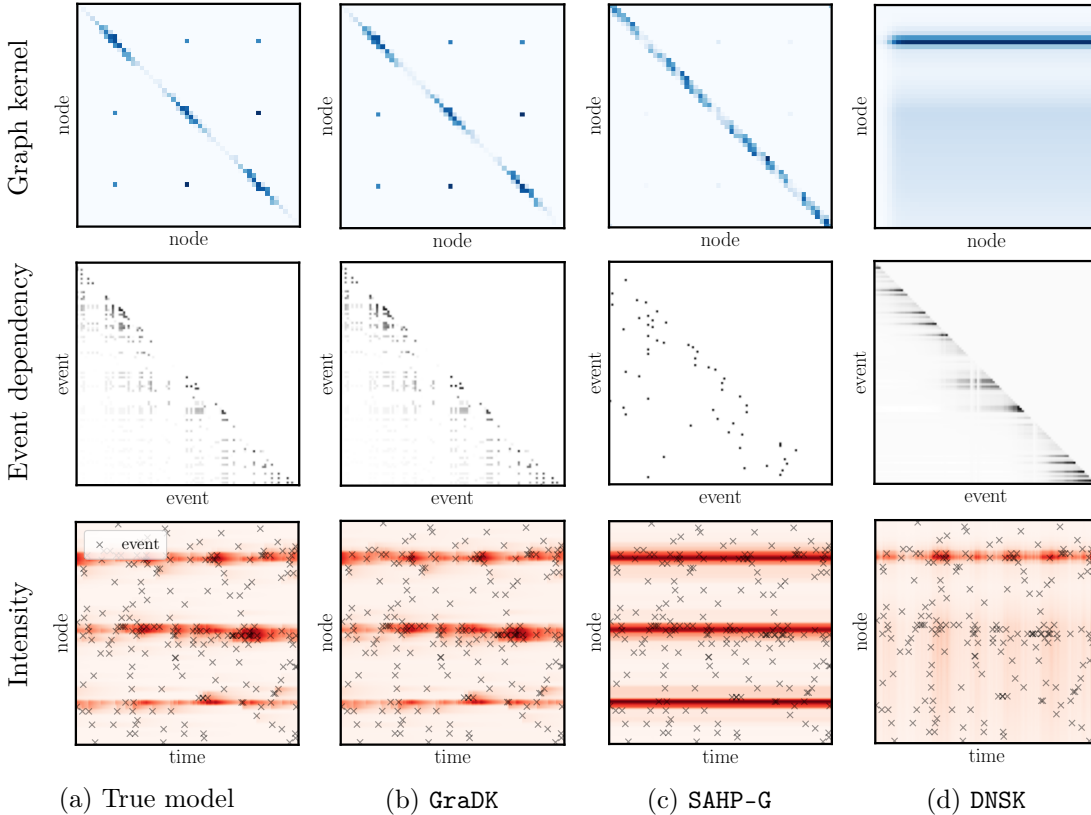


Figure 2: Graph kernel, inter-event dependence, and conditional intensity recovery for the 50-node synthetic data set. The first column reflects the ground truth, while the subsequent columns reflect the results obtained by **GraDK** (our method), **SAHP-G**, and **DNSK**, respectively.

is characterized by the influence kernel (2) in **GraDK**, **DNSK**, and the true model. For **SAHP-G**, the event dependency is indicated by the scaled self-attention weight (Equation 10 [40]). While **SAHP-G** is capable of discovering long-term dependencies, the decaying influence of recent events is not represented. The event dependency of **DNSK** does well to capture the decaying influence of recent events, but fails to capture long-term effects by certain event types. Our method learns both of these features, capturing long-term dependence and decaying influence similar to that of the true model. Similarly, the second row of Figure 3 shows the inter-event dependency for the data on the 16-node ring graph with 2-hop influence. Still, **SAHP-G** erroneously presents some long-term effects and **DNSK** fails to capture intermediate-time influence from past events, whereas **GraDK** captures the influence at all proper timescales.

Predictive ability. The superior predictive performance of **GraDK** is further substantiated through a comprehensive evaluation. Apart from assessing the fitted log-likelihood (ℓ) of the testing data, for each data set, we generate 100 event sequences using each learned model (one of three independent runs) and provide two metrics: (i) the mean absolute error of predicted event frequency (*Time MAE*) compared to that in the testing data, and (ii) the Kullback–Leibler

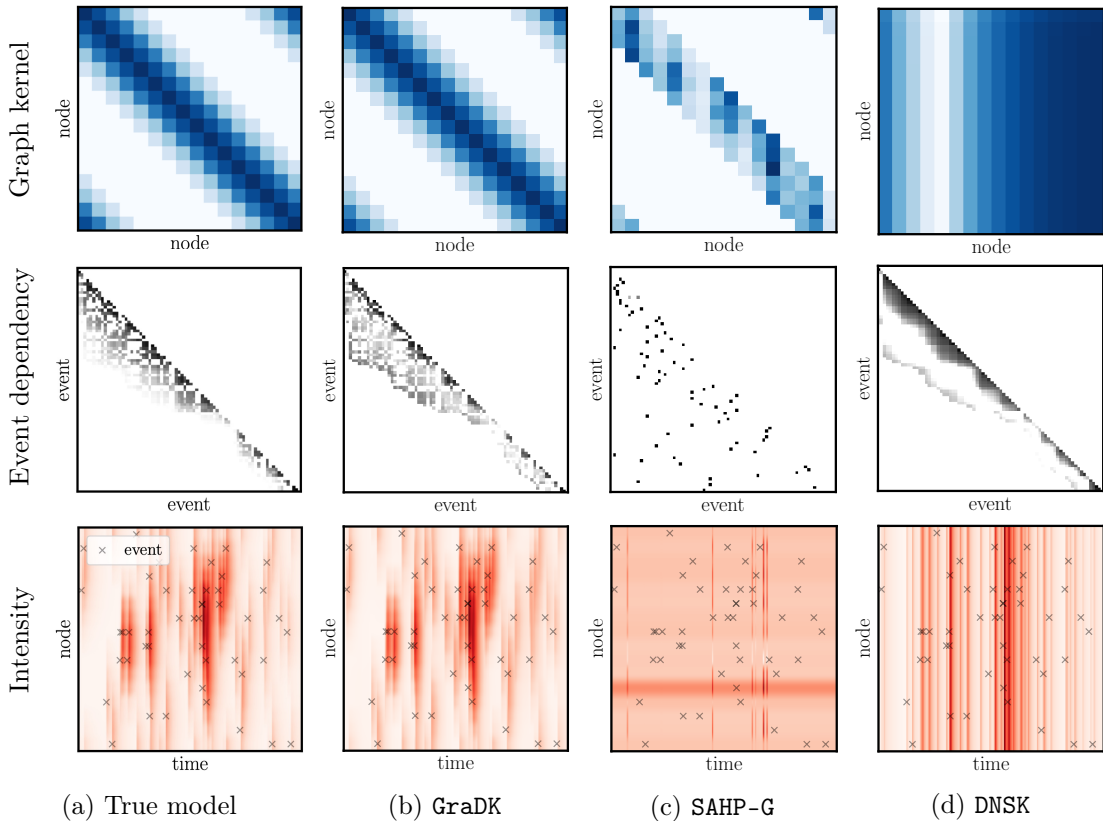


Figure 3: Graph kernel, inter-event dependence, and conditional intensity recovery for the 16-node synthetic data set with 2-hop graph influence. The first column reflects the ground truth, while the subsequent columns reflect the results obtained by **GraDK**, **SAHP-G**, and **DNSK**, respectively.

Divergence of predicted event types (*Type KLD*), which compares the empirical distributions of event types (nodes) in the testing data and generated sequences. These metrics, proposed in a previous study [17], reflect the model’s predictive capacity for future events, as opposed to individual event prediction accuracy, which tends to be noisy when applied to large graphs. The quantitative results in Table 1 demonstrate that **GraDK** method excels in fitting sequential data on a latent graph. It achieves the highest log-likelihood across all datasets and significantly outperforms all baseline methods in predicting future events, which holds immense importance within the domain of point process modeling.

4.2 Real data

Traffic congestion data. The Georgia Department of Transportation (GDOT) provides traffic volume data for sensors embedded on roads and highways in the state. We have access to such data for 5 sensors at the interchange of interstates 75 and 85 in Midtown Atlanta from September 2018 to March 2019. Traffic volume is measured in 15-minute intervals, and congestion events are detected when the traffic count exceeds the third quartile of the daily traffic volume. The result is

Table 1: Synthetic data results.

Model	3-node graph with negative influence			16-node graph with 2-hop influence			50-node graph		
	Testing ℓ	Time MAE	Type KLD	Testing ℓ	Time MAE	Type KLD	Testing ℓ	Time MAE	Type KLD
RMTTP	-3.473 _(0.087)	0.528	0.093	-7.239 _(0.193)	0.301	0.142	-27.915 _(1.251)	37.666	0.103
FullyNN	-2.086 _(0.009)	0.291	0.006	-3.347 _(0.018)	0.198	0.018	-1.736 _(0.019)	13.295	0.058
DNSK	-2.127 _(0.003)	0.149	0.012	-3.005 _(0.002)	0.085	0.002	-1.165 _(0.003)	1.074	0.076
THP-S	-2.089 _(0.008)	0.413	0.006	-3.079 _(0.004)	0.108	0.011	-1.091 _(0.005)	3.940	0.019
SAHP-G	-2.113 _(0.005)	0.172	0.003	-3.036 _(0.008)	0.155	0.005	-1.099 _(0.004)	1.119	0.014
GraDK	-2.055 _(0.003)	0.123	0.001	-2.990 _(0.002)	0.054	<0.001	-1.058 _(0.002)	0.453	0.003

*Numbers in parentheses are standard errors for three independent runs.

3,830 events which are split into 24-hour trajectories (with an average of 24 events per day). The latent graph connects 5 sensors based on the flow of traffic and proximity.

Wildfire data. The California Public Utilities Commission (CPUC) maintains a large-scale multi-modal wildfire incident dataset. We extract a total of 2,428 wildfire occurrences in California from 2014 to 2019. The latitude-longitude coordinates of incidents are bounded by the rectangular region $[34.51, -123.50] \times [40.73, -118.49]$. Note that the majority of the region has no fire in the 5-year horizon due to the fact that fire incidents are likely to cluster in space. Therefore, we apply the K-means algorithm to extract 25 clusters of wildfire incidents. The latent graph is constructed such that each node represents one cluster and is connected to geographically adjacent nodes. The entire dataset is split into one-year sequences with an average length of 436 events.

Theft data. The proprietary crime data collected by the police department in Valencia, Spain records the crime incidents that happened from 2015 to 2019, including incident location, crime category, and distance to various landmarks within the city. We analyze 9,372 sustracciones (smooth thefts) that happened near 52 pubs within the Valencia city area. The graph is constructed from the street network, with each node representing a pub. Two pubs are connected if the distance between them along the street is less than 1 km. Each sustraccion is assigned to the closest pub. We partition the data into quarter-year-long sequences with an average length of 469 events.

Results in Table 2 underscore the efficacy of the GraDK approach in acquiring knowledge about graph point processes across a diverse array of real-world domains, including a small traffic graph of 5 nodes up to a large crime network of 52 nodes. These settings encompass diverse event dependency dynamics, as the influence mechanisms include infrastructure (roadways for traffic patterns), nature (weather and climate for wildfire patterns), and social dynamics (criminal behavior for theft patterns). Despite the complexity inherent in these scenarios, our method excels in providing a robust framework capable of capturing the intricate dependencies and facilitating accurate predictions, demonstrated by the low Time MAE and Type KLD from our method in each setting, which is better than or comparable to the best baselines in each of the three real data sets.

In Figure 4, the learned graph kernels of (a) GraDK, (b) SAHP-G, and (c) DNSK are visualized for the theft data set. The second panel reveals that SAHP-G learns a very noisy graph kernel, resulting in a conditional intensity that depends very slightly on inter-event influence. In fact, this approach learns a homogeneous Poisson process for each node with a relatively high likelihood.

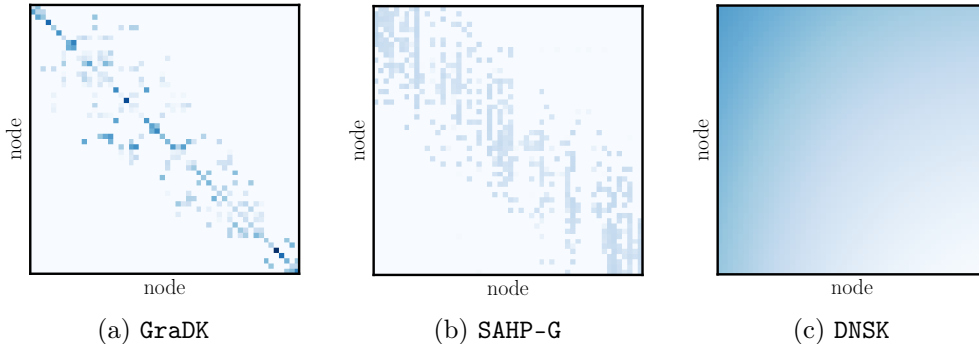


Figure 4: Learned graph kernels for theft data set. The columns present the recovered kernels on the theft data set of GraDK, SAHP-G, and DNSK, respectively.

Table 2: Real data results.

Model	Traffic congestion			Wildfire			Theft		
	Testing ℓ	Time MAE	Type KLD	Testing ℓ	Time MAE	Type KLD	Testing ℓ	Time MAE	Type KLD
RMTPP	-5.197 _(0.662)	2.348	0.021	-6.155 _(1.589)	1.180	0.178	-11.496 _(1.474)	5.871	0.124
FullyNN	-3.292 _(0.108)	0.511	0.012	-4.717 _(0.119)	0.817	0.026	-3.468 _(0.068)	6.457	1.169
DNSK	-2.401 _(0.011)	0.934	0.010	-3.706 _(0.008)	0.711	0.083	-3.347 _(0.012)	0.507	0.177
THP-S	-2.254 _(0.007)	0.378	0.003	-4.523 _(0.018)	1.183	0.134	-2.982 _(<0.001)	0.739	0.189
SAHP-G	-2.453 _(0.013)	0.729	0.021	-3.919 _(0.040)	0.551	0.032	-2.970 _(0.032)	0.464	0.096
GraDK	-2.286 _(0.002)	0.314	0.001	-3.625 _(0.009)	0.358	0.024	-3.039 _(0.011)	1.052	0.082

*Numbers in parentheses are standard errors for three independent runs.

The third panel shows that DNSK fails to present meaningful or discernible patterns of self-influence or event-type interdependence. Lastly, GraDK captures self-influence and inter-node dependencies with the aid of the flexible influence kernel, indicating the complex inhomogeneous dynamics in real data with great model interpretability.

5 Discussion

We develop a novel deep kernel for graph point processes using graph convolution filters in convolutional GNNs. This construction permits the efficient learning of intricate and non-stationary event dynamics on a latent graph structure. The modeling of the kernel enhances model interpretability, as one can parse the learned kernel to understand event type interdependence. We empirically demonstrate that our approach outperforms existing methods in terms of dependency recovery and event prediction across various data settings, including large graph structures and those with multi-hop influence.

While our approach adopts convolutional GNNs via local filters, we provide a flexible framework that can conveniently incorporate alternative GNN architectures. Extensions can explore the advantages of such other architectures, *e.g.*, recurrent graph neural networks [16] and graph attention networks [35]. Furthermore, our method has the potential to be integrated into different problem formulations to serve diverse research objectives, such as Granger causality for point processes and latent graph structure inference without access to the existing graph.

Acknowledgement

The work is supported by NSF DMS-2134037. Z.D., M.R. and Y.X. are partially supported by an NSF CAREER CCF-1650913, NSF DMS-2134037, CMMI-2015787, CMMI-2112533, DMS-1938106, and DMS-1830210. X.C. is partially supported by NSF CAREER DMS-2237842, Simons Foundation 814643, and the Alfred P. Sloan Foundation.

References

- [1] Atwood, J. and Towsley, D. (2016). Diffusion-convolutional neural networks. *Advances in neural information processing systems*, 29.
- [2] Bhattacharjya, D., Subramanian, D., and Gao, T. (2018). Proximal graphical event models. *Advances in Neural Information Processing Systems*, 31.
- [3] Bianchi, F. M., Grattarola, D., Livi, L., and Alippi, C. (2021). Graph neural networks with convolutional arma filters. *IEEE transactions on pattern analysis and machine intelligence*, 44(7):3496–3507.
- [4] Brody, S., Alon, U., and Yahav, E. (2021). How attentive are graph attention networks? *arXiv preprint arXiv:2105.14491*.
- [5] Bruna, J., Zaremba, W., Szlam, A., and LeCun, Y. (2013). Spectral networks and locally connected networks on graphs. *arXiv preprint arXiv:1312.6203*.
- [6] Cai, B., Zhang, J., and Guan, Y. (2022). Latent network structure learning from high-dimensional multivariate point processes. *Journal of the American Statistical Association*, pages 1–14.
- [7] Cai, L., Chen, Z., Luo, C., Gui, J., Ni, J., Li, D., and Chen, H. (2021). Structural temporal graph neural networks for anomaly detection in dynamic graphs. In *Proceedings of the 30th ACM international conference on Information & Knowledge Management*, pages 3747–3756.
- [8] Cheng, X., Miao, Z., and Qiu, Q. (2020). Graph convolution with low-rank learnable local filters. *arXiv preprint arXiv:2008.01818*.
- [9] Daley, D. J. and Vere-Jones, D. (2007). *An introduction to the theory of point processes: volume II: general theory and structure*. Springer Science & Business Media.
- [10] Defferrard, M., Bresson, X., and Vandergheynst, P. (2016). Convolutional neural networks on graphs with fast localized spectral filtering. *Advances in neural information processing systems*, 29.
- [11] Deng, A. and Hooi, B. (2021). Graph neural network-based anomaly detection in multivariate time series. *Proceedings of the AAAI conference on artificial intelligence*, 35(5):4027–4035.
- [12] Dong, Z., Cheng, X., and Xie, Y. (2022). Spatio-temporal point processes with deep non-stationary kernels. *arXiv preprint arXiv:2211.11179*.

- [13] Du, N., Dai, H., Trivedi, R., Upadhyay, U., Gomez-Rodriguez, M., and Song, L. (2016). Recurrent marked temporal point processes: Embedding event history to vector. In *Proceedings of the 22nd ACM SIGKDD international conference on knowledge discovery and data mining*, pages 1555–1564.
- [14] Dwivedi, V. P. and Bresson, X. (2020). A generalization of transformer networks to graphs. *arXiv preprint arXiv:2012.09699*.
- [15] Hawkes, A. G. (1971). Spectra of some self-exciting and mutually exciting point processes. *Biometrika*, 58(1):83–90.
- [16] Ioannidis, V. N., Marques, A. G., and Giannakis, G. B. (2019). A recurrent graph neural network for multi-relational data. In *ICASSP 2019-2019 IEEE International Conference on Acoustics, Speech and Signal Processing (ICASSP)*, pages 8157–8161. IEEE.
- [17] Juditsky, A., Nemirovski, A., Xie, L., and Xie, Y. (2020). Convex parameter recovery for interacting marked processes. *IEEE Journal on Selected Areas in Information Theory*, 1(3):799–813.
- [18] Kingma, D. P. and Ba, J. (2014). Adam: A method for stochastic optimization. *arXiv preprint arXiv:1412.6980*.
- [19] Kipf, T. N. and Welling, M. (2016). Semi-supervised classification with graph convolutional networks. *arXiv preprint arXiv:1609.02907*.
- [20] Linderman, S. and Adams, R. (2014). Discovering latent network structure in point process data. In *International conference on machine learning*, pages 1413–1421. PMLR.
- [21] Longa, A., Lachi, V., Santin, G., Bianchini, M., Lepri, B., Lio, P., Scarselli, F., and Passerini, A. (2023). Graph neural networks for temporal graphs: State of the art, open challenges, and opportunities. *arXiv preprint arXiv:2302.01018*.
- [22] Mei, H. and Eisner, J. M. (2017). The neural Hawkes process: A neurally self-modulating multivariate point process. *Advances in neural information processing systems*, 30.
- [23] Mercer, J. (1909). Xvi. functions of positive and negative type, and their connection the theory of integral equations. *Philosophical transactions of the royal society of London. Series A, containing papers of a mathematical or physical character*, 209(441-458):415–446.
- [24] Mollenhauer, M., Schuster, I., Klus, S., and Schütte, C. (2020). Singular value decomposition of operators on reproducing kernel Hilbert spaces. In *Advances in Dynamics, Optimization and Computation: A volume dedicated to Michael Dellnitz on the occasion of his 60th birthday*, pages 109–131. Springer.
- [25] Ogata, Y. (1988). Statistical models for earthquake occurrences and residual analysis for point processes. *Journal of the American Statistical Association*, 83(401):9–27.

- [26] Okawa, M., Iwata, T., Tanaka, Y., Toda, H., Kurashima, T., and Kashima, H. (2021). Dynamic Hawkes processes for discovering time-evolving communities’ states behind diffusion processes. In *Proceedings of the 27th ACM SIGKDD Conference on Knowledge Discovery & Data Mining*, pages 1276–1286.
- [27] Omi, T., Aihara, K., et al. (2019). Fully neural network based model for general temporal point processes. *Advances in neural information processing systems*, 32.
- [28] Rampášek, L., Galkin, M., Dwivedi, V. P., Luu, A. T., Wolf, G., and Beaini, D. (2022). Recipe for a general, powerful, scalable graph transformer. *Advances in Neural Information Processing Systems*, 35:14501–14515.
- [29] Reinhart, A. (2018). A review of self-exciting spatio-temporal point processes and their applications. *Statistical Science*, 33(3):299–318.
- [30] Shang, J. and Sun, M. (2019). Geometric Hawkes processes with graph convolutional recurrent neural networks. In *Proceedings of the AAAI conference on artificial intelligence*, volume 33, pages 4878–4885.
- [31] Shchur, O., Biloš, M., and Günnemann, S. (2019). Intensity-free learning of temporal point processes. *arXiv preprint arXiv:1909.12127*.
- [32] Sulem, D., Kenlay, H., Cucuringu, M., and Dong, X. (2022). Graph similarity learning for change-point detection in dynamic networks. *arXiv preprint arXiv:2203.15470*.
- [33] Tang, J., Li, J., Gao, Z., and Li, J. (2022). Rethinking graph neural networks for anomaly detection. In *International Conference on Machine Learning*, pages 21076–21089. PMLR.
- [34] Vaswani, A., Shazeer, N., Parmar, N., Uszkoreit, J., Jones, L., Gomez, A. N., Kaiser, Ł., and Polosukhin, I. (2017). Attention is all you need. *Advances in neural information processing systems*, 30.
- [35] Velickovic, P., Cucurull, G., Casanova, A., Romero, A., Lio, P., Bengio, Y., et al. (2017). Graph attention networks. *stat*, 1050(20):10–48550.
- [36] Wu, W., Liu, H., Zhang, X., Liu, Y., and Zha, H. (2020a). Modeling event propagation via graph biased temporal point process. *IEEE Transactions on Neural Networks and Learning Systems*.
- [37] Wu, Z., Pan, S., Chen, F., Long, G., Zhang, C., and Philip, S. Y. (2020b). A comprehensive survey on graph neural networks. *IEEE transactions on neural networks and learning systems*, 32(1):4–24.
- [38] Xia, W., Li, Y., and Li, S. (2022). Graph neural point process for temporal interaction prediction. *IEEE Transactions on Knowledge and Data Engineering*.
- [39] Yang, C., Mei, H., and Eisner, J. (2021). Transformer embeddings of irregularly spaced events and their participants. *arXiv preprint arXiv:2201.00044*.

- [40] Zhang, Q., Lipani, A., Kirnap, O., and Yilmaz, E. (2020a). Self-attentive hawkes process. In *International conference on machine learning*, pages 11183–11193. PMLR.
- [41] Zhang, Q., Lipani, A., and Yilmaz, E. (2021). Learning neural point processes with latent graphs. In *Proceedings of the Web Conference 2021*, pages 1495–1505.
- [42] Zhang, R., Hao, Y., Yu, D., Chang, W.-C., Lai, G., and Yang, Y. (2020b). Correlation-aware change-point detection via graph neural networks. In *Neural Information Processing: 27th International Conference, ICONIP 2020, Bangkok, Thailand, November 23–27, 2020, Proceedings, Part III 27*, pages 555–567. Springer.
- [43] Zhang, Y. and Yan, J. (2021). Neural relation inference for multi-dimensional temporal point processes via message passing graph. In *IJCAI*, pages 3406–3412.
- [44] Zhu, H. and Koniusz, P. (2021). Simple spectral graph convolution. In *International conference on learning representations*.
- [45] Zhu, S., Li, S., Peng, Z., and Xie, Y. (2021). Imitation learning of neural spatio-temporal point processes. *IEEE Transactions on Knowledge and Data Engineering*, 34(11):5391–5402.
- [46] Zhu, S. and Xie, Y. (2022). Spatiotemporal-textual point processes for crime linkage detection. *The Annals of Applied Statistics*, 16(2):1151–1170.
- [47] Zuo, S., Jiang, H., Li, Z., Zhao, T., and Zha, H. (2020). Transformer hawkes process. In *International conference on machine learning*, pages 11692–11702. PMLR.

Appendix

A Incorporation of localized graph filters in graph kernel

We provide the details of incorporating different localized graph filters in graph convolutions into our proposed graph basis kernel, including the model formulation and complexity (number of trainable parameters). A graph convolution layer maps the input node feature X to the output feature Y . Particularly, for the graph convolutions in the graph neural networks discussed in Section 3.3, we have:

- (1) *Chebnet*[10]: The filtering operation in Chebnet is defined as

$$Y = \sum_{r=0}^{R-1} \theta_r T_r(\tilde{L})X,$$

where T_r is the Chebyshev polynomial of order r evaluated at the scaled and normalized graph Laplacian $\tilde{L} = 2L/\lambda_{\max} - I$, where $L = I - D^{-1/2}AD^{-1/2}$, D is the degree matrix, A is the adjacency matrix, and λ_{\max} is the largest eigenvalue of L .

We let $B_r = T_{r-1}(\tilde{L}) \in \mathbb{R}^{|V| \times |V|}$, which can be computed by the recurrence relation of Chebyshev polynomial $B_r = 2LB_{r-1} - B_{r-2}$. Since $\{B_r\}_{r=1}^R$ are calculated by the graph Laplacian, the trainable parameters are polynomial coefficients (in our case, the weights that combine basis kernels) of $\mathcal{O}(R)$.

- (2) *L3Net*[8]: In L3Net, the graph convolution layer for single channel graph signal is specified as (omitting the bias, non-linear mapping)

$$Y = \sum_{r=1}^R a_r B_r^{(o_r)}(v', v) X.$$

Each $B_r^{(o_r)}(v', v) \neq 0$ only if $v \in N_{v'}^{(o_r)}$.

In our model, we choose an integer o_r for each B_r and formulate them the same way in L3Net. Thus, each $B_r(v', v)$ models the influence from v' to its o_r -th order neighbors on the graph. All bases $\{B_r\}_{r=1}^R$ are learnable. Assuming the average number of neighbors of graph nodes is C , the total number of trainable parameters is of $\mathcal{O}(RC|V|)$.

- (3) *GAT*[35]: Considering GAT with R attention heads, the graph convolution operator in one layer can be written as

$$Y = \sum_{r=1}^R \mathcal{A}^{(r)} X \Theta_r, \quad \mathcal{A}_{v',v}^{(r)} = \frac{e^{c_{v',v}^{(r)}}}{\sum_{v \in N_{v'}^{(1)}} e^{c_{v',v}^{(r)}}}, \quad c_{v',v}^{(r)} = \sigma((a^{(r)})^\top [W^{(r)} X_{v'} || W^{(r)} X_v]).$$

Here $\{a^{(r)}, W^{(r)}\}_{r=1}^R$ are trainable model parameters, and $\Theta_r = W^{(r)} C^{(r)}$, where $C^{(r)}$ is a fixed matrix for concatenating outputs from R attention heads. Mask attention is applied to inject the graph structure, that is, $\mathcal{A}_{v',v}^{(r)} \neq 0$ only when $v \in N_{v'}^{(1)}$.

Therefore, each $B_r(v', v)$ in our graph basis kernel can be a learnable localized graph filter with positive entries and column-wise summation normalized to one to mimic the affinity matrix $\mathcal{A}^{(r)}$. When global attention is allowed, *i.e.*, every node can attend on every other node), the number of trainable parameters is of $\mathcal{O}(R|V|^2)$. When mask attention is applied (which is commonly used in GAT), the total number of trainable parameters is $\mathcal{O}(RC|V|)$.

- (4) *GPS Graph Transformer* [28]: At each layer of GPS Graph Transformer, the graph node features are updated by aggregating the output of a message-passing graph neural network (MPNN) layer and a global attention layer. Assuming a sum aggregator in the MPNN layer, the filter operation can be expressed as

$$Y = \sum_{r=1}^R \left(\mathcal{A}^{(r)} X W_1^{(r)} + X W_2^{(r)} \right) C^{(r)}.$$

Here $\mathcal{A}^{(r)}$ is the affinity matrix in the attention layer, and $W_1^{(r)}, W_2^{(r)}$ are weight matrices in the attention layer and MPNN layer, respectively. The fixed matrices $\{C^{(r)}\}$ concatenate the R attention heads and MPNN layers.

We can integrate such a GPS Graph Transformer structure by introducing $2R$ localized graph filter bases. For each r , B_r takes the form of a learnable affinity matrix, and $B_{2r} = A$, where A is the graph adjacency matrix. Here $\{B_r\}_{r=1}^R$ are learnable and $\{B_r\}_{r=R+1}^{2R}$ are fixed. The total number of trainable parameters with mask attention adopted is of $\mathcal{O}(RC|V|)$.

B Efficient model computation

The computational complexity associated with calculating the model log-likelihood has consistently posed a limitation for neural point processes. Due to the existence of neural networks, numerical

integration is widely adopted for estimating the intractable model log-likelihood. However, this approach is computationally demanding. Specifically, we identify three distinct components in our optimization objective (5) as log-summation, integral, and log-barrier, respectively. For the simplicity of presentation, we consider that there is one event sequence $\{(t_i, v_i)\}_{i=1}^n$ in \mathcal{S} with a total number of n events. The computational complexity of evaluating the neural network is of $\mathcal{O}(n^2)$ for the log-summation and log-barrier terms, and $\mathcal{O}(K|V|n)$ for the integral, where K is the number of sampled points for the numerical integration over the time span.

To address these challenges, we adopt a domain discretization strategy that allows for the efficient computation of the optimization objective $\mathcal{L}(\theta)$, resulting in computational complexity of $\mathcal{O}(n)$. In particular, we introduce a uniform grid \mathcal{U}_t over time horizon $[0, T]$, and the computation for each term can be carried out as follows:

- *Log-summation.* We plug in the influence kernel (3) to the log-summation term and have

$$\sum_{i=1}^n \log \lambda(t_i, v_i) = \sum_{i=1}^n \log \left(\mu + \sum_{t_j < t_i} \sum_{r=1}^R \sum_{l=1}^L \alpha_{lr} \psi_l(t_j) \varphi_l(t_i - t_j) B_r(v_j, v_i) \right).$$

Each ψ_l is only evaluated at event times $\{t_i\}_{i=1}^n$. To prevent redundant evaluations of the function φ_l for every pair of event times (t_i, t_j) , we restrict the evaluation of φ_l on the grid \mathcal{U}_t . By adopting linear interpolation between two neighboring grid points of $t_i - t_j$, we can determine the value of $\varphi_l(t_i - t_j)$. In practice, the influence of past events is limited to a finite range, which can be governed by a hyperparameter τ_{\max} . Consequently, we can let $\varphi_l(\cdot) = 0$ when $t_i - t_j > \tau_{\max}$ without any neural network evaluation. The computation of $B_r(v_j, v_i)$ is accomplished using matrix indexing, a process that exhibits constant computational complexity when compared to the evaluation of neural networks.

- *Integral.* The efficient computation of the integral benefits from the formulation of our conditional intensity function. We have

$$\begin{aligned} \sum_{v \in V} \int_0^T \lambda(t, v) dt &= \mu |V| T + \sum_{i=1}^n \sum_{v \in V} \int_0^T I(t_i < t) k(t_i, t, v_i, v) dt \\ &= \mu |V| T + \sum_{i=1}^n \sum_{r=1}^R \sum_{v=1}^V B_r(v_i, v) \sum_{l=1}^L \alpha_{rl} \psi_l(t_i) \int_0^{T-t_i} \varphi_l(t) dt. \end{aligned}$$

Similarly, the evaluations of $B_r(v_i, v)$ are the extractions of corresponding entries in the matrices, and ψ_l is only evaluated at event times $\{t_i\}_{i=1}^n$. We leverage the evaluations of φ_l on the grid \mathcal{U}_t to facilitate the computation of the integral of φ_l . Let $F_l(t) := \int_0^t \varphi_l(\tau) d\tau$. The value of F_l on j -th grid point in \mathcal{U}_t equals the cumulative sum of φ_l from the first grid point up to the j -th point, multiplied by the grid width. Then $F_l(T - t_i)$ can be computed by the linear interpolation of values of F_l at two adjacent grid points of $T - t_i$.

- *Log-barrier.* The computation can be carried out similarly to the computation of the log-summation term by replacing (t_i, v_i) with (t, v) where $t \in \mathcal{U}_{\text{bar}, t}, v \in V$.

In summary, the evaluation of $\{\psi_l\}_{l=1}^L$ has a complexity of $\mathcal{O}(Ln)$, while the evaluation of $\{\varphi_l\}_{l=1}^L$ requires $\mathcal{O}(L|\mathcal{U}_t|)$ complexity. On the other hand, $\{B_r\}_{r=1}^R$ are computed with $\mathcal{O}(1)$ complexity. Therefore, the total complexity of our model computation is $\mathcal{O}(n + |\mathcal{U}_t|)$. Moreover, the grid selection in practice is flexible, striking a balance between learning accuracy and efficiency. For instance, the number of grid points in \mathcal{U}_t and $\mathcal{U}_{\text{bar},t}$ can be both chosen around $\mathcal{O}(n)$, leading to an overall computational complexity of $\mathcal{O}(n)$. It is worth noting that all the evaluations of neural networks and localized filter bases can be implemented beforehand, and the optimization objective (5) is efficiently calculated using basic numerical operations.

C Algorithm

Algorithm 1 Model learning

Input: Training set X , batch size M , epoch number E , learning rate γ , constant $a > 1$ to update w in (5).

Initialization: model parameter θ_0 , first epoch $e = 0$, $s = s_0$. Small enough b_e to lower-bound the conditional intensity.

while $e < E$ **do**

 Set $b_{temp} = 0$.

for each batch with size M **do**

 1. Compute $\ell(\theta)$, $\{\lambda(t_{c_t}, s_{c_s})\}_{c_t=1, \dots, |\mathcal{U}_{\text{bar},t}|, c_s=1, \dots, |V|}$.

 2. Compute $\mathcal{L}(\theta) = -\ell(\theta) + \frac{1}{w}p(\theta, b_e)$.

 3. Update $\theta_{e+1} \leftarrow \theta_e - \gamma \frac{\partial \mathcal{L}}{\partial \theta_e}$.

 4. Set $b_{temp} = \min \left\{ \min \{ \{\lambda(t_{c_t}, s_{c_s})\}_{c_t=1, \dots, |\mathcal{U}_{\text{bar},t}|, c_s=1, \dots, |\mathcal{U}_{\text{bar},s}|} - \epsilon, b_{temp} \right\}$, where ϵ is a small value to guarantee logarithm feasibility.

end for

$e \leftarrow e + 1, w \leftarrow w \cdot a, b_e = b_{temp}$

end while

D Experimental details and additional results

In this section, we give details regarding the experiments in Section 4, including a description of the ground truth point process models for synthetic data, latent graph structures for real data, experimental setup, and additional results.

D.1 Data description

Our experiments are implemented using three synthetic and three real-world data sets.

Synthetic data. We provide a detailed description of the ground truth kernels and latent graph structures we used for synthetic data generation:

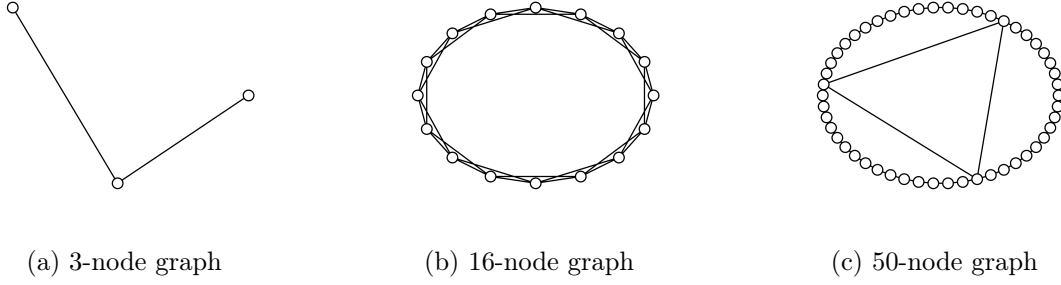


Figure A.1: Latent graph structures for the synthetic data sets. From left to right, the graphs correspond to the 3-node graph, the 16-node ring graph, and the 50-node graph in synthetic data set 1, 2, and 3, respectively.

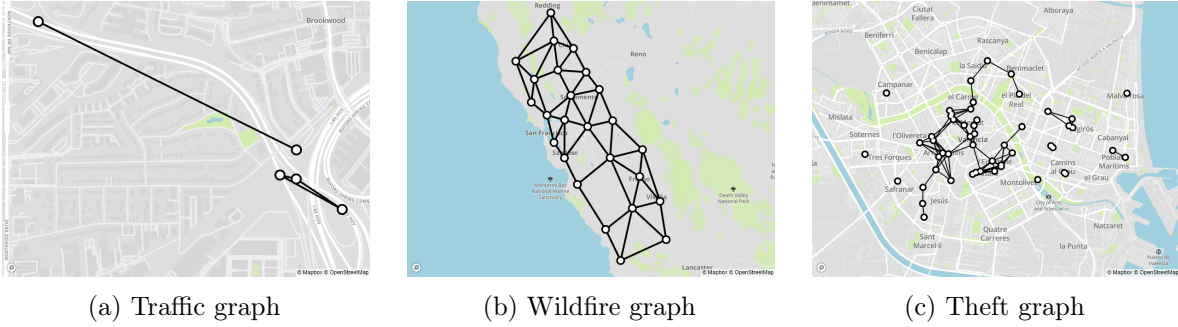


Figure A.2: Latent graph structures for the real data sets. From left to right, the graphs correspond to the ones in Atlanta traffic congestion data, the California wildfire data, and the Valencia sustraccion (theft) data.

- (i) 3 nodes with non-stationary temporal kernel and 1-hop (positive and negative) graph influence:

$$k(t', t, v', v) = 1.5(0.5 + 0.5 \cos(0.2t'))e^{-2(t-t')} \left(0.5B_1^{(0)}(v', v) + 0.2B_2^{(1)}(v', v) \right),$$

where $B_1^{(0)} = \text{diag}(0.5, 0.7, 0.5)$, $B_2^{(1)}(2, 1) = -0.2$, and $B_2^{(1)}(2, 3) = 0.4$.

- (ii) 16 nodes with non-stationary temporal kernel and 2-hop graph influence:

$$k(t', t, v', v) = 1.5(0.5 + 0.5 \cos(0.2t'))e^{-2(t-t')} \left(0.2B_1^{(0)}(v', v) - 0.3B_2^{(1)}(v', v) + 0.1B_3^{(2)}(v', v) \right),$$

such that $(0.2B_1^{(0)} - 0.3B_2^{(1)} + 0.1B_3^{(2)}) = (0.2I - 0.3\tilde{L} + 0.1(2\tilde{L}^2 - I))$. Here \tilde{L} is the scaled and normalized graph Laplacian defined in Section 3.3. This graph influence kernel is visualized in the top row of Figure 3(a).

- (iii) 50 nodes with exponentially decaying temporal kernel: $g(t', t) = 2e^{-2(t-t')}$. The graph kernel is constructed such that the influence follows a Gaussian density (with 3 modes) along the diagonal of the graph influence kernel with random noise in addition to off-ring influence. The true graph kernel is visualized in the top row of Figure 2(a).

Table A.1: Training hyper-parameters for the baselines.

Model	3-node synthetic		16-node synthetic		50-node synthetic		Traffic		Wildfire		Theft	
	Learning Rate	Batch Size	Learning Rate	Batch Size	Learning Rate	Batch Size	Learning Rate	Batch Size	Learning Rate	Batch Size	Learning Rate	Batch Size
RMTPP	10^{-3}	32	10^{-3}	32	10^{-3}	32	10^{-3}	32	10^{-3}	2	10^{-3}	2
FullyNN	10^{-2}	100	10^{-2}	100	10^{-2}	100	10^{-3}	50	10^{-3}	20	10^{-3}	100
DNSK	10^{-1}	32	10^{-1}	32	10^{-1}	32	10^{-1}	32	10^{-1}	2	10^{-1}	2
THP-S	10^{-3}	32	10^{-3}	32	10^{-3}	32	10^{-3}	64	10^{-3}	2	10^{-3}	2
SAHP-G	10^{-4}	32	10^{-4}	32	10^{-4}	32	10^{-4}	32	10^{-3}	2	10^{-3}	2

The latent graph structures for these three synthetic data experiments can be found in Figure A.1.

Real data. We also apply the model to three real data sets across different real-world settings. The latent graph structures overlaid on the real-world geography are displayed in Figure A.2 for the Atlanta traffic congestion, California wildfire, and Valencia theft data.

D.2 Detailed experimental setup

For the baseline of RMTPP, we test the dimension of $\{32, 64, 128\}$ for the hidden embedding in RNN and choose an embedding dimension of 32 in the experiments. For FullyNN, we set the embedding dimension to be 64 and use a fully-connected neural network with two hidden layers of width 64 for the cumulative hazard function, as the default ones in the original paper. The dimension of input embedding is set to 10. For DNSK, we adopt the structure for the marked point processes, and set the rank of temporal basis and mark basis to 1 and 3. THP-S and SAHP-G use the default parameters from their respective code implementations. The GraDK method uses a rank 1 basis for the temporal kernel and a rank 2 basis for the graph kernel (except in the ring graph with 2-hop influence, which uses a rank 3 basis). The ranks of the bases in our experiments correspond to zero- (self-), one-, and two-hop influence. The temporal kernel basis functions are fully-connected neural networks with two hidden layers of size 32. Learning rate and batch size parameters are provided for each baseline and experiment in Table A.1.

D.3 Additional experimental results

Synthetic data. Figure A.3 presents the kernel and intensity recovery results for the synthetic data set 1 generated by a non-stationary temporal kernel and a 3-node-graph kernel with inhibitive influence. The recovery outcomes demonstrate the efficacy of our proposed model in characterizing the temporal and graph-based dependencies among events, as evident from the first and second rows of the figure. Moreover, the results emphasize the capability of our model, GraDK, to effectively capture the inhibitive effects of past events. In contrast, the event dependencies represented by the normalized positive attention weights in SAHP solely capture the triggering intensity of past events without accounting for inhibitive influences.

Real data. We visualize the learned graph kernels by GraDK, SAHP, and DNSK on traffic and wildfire data in Figure A.4. Our approach is able to learn intense graph signals with complex

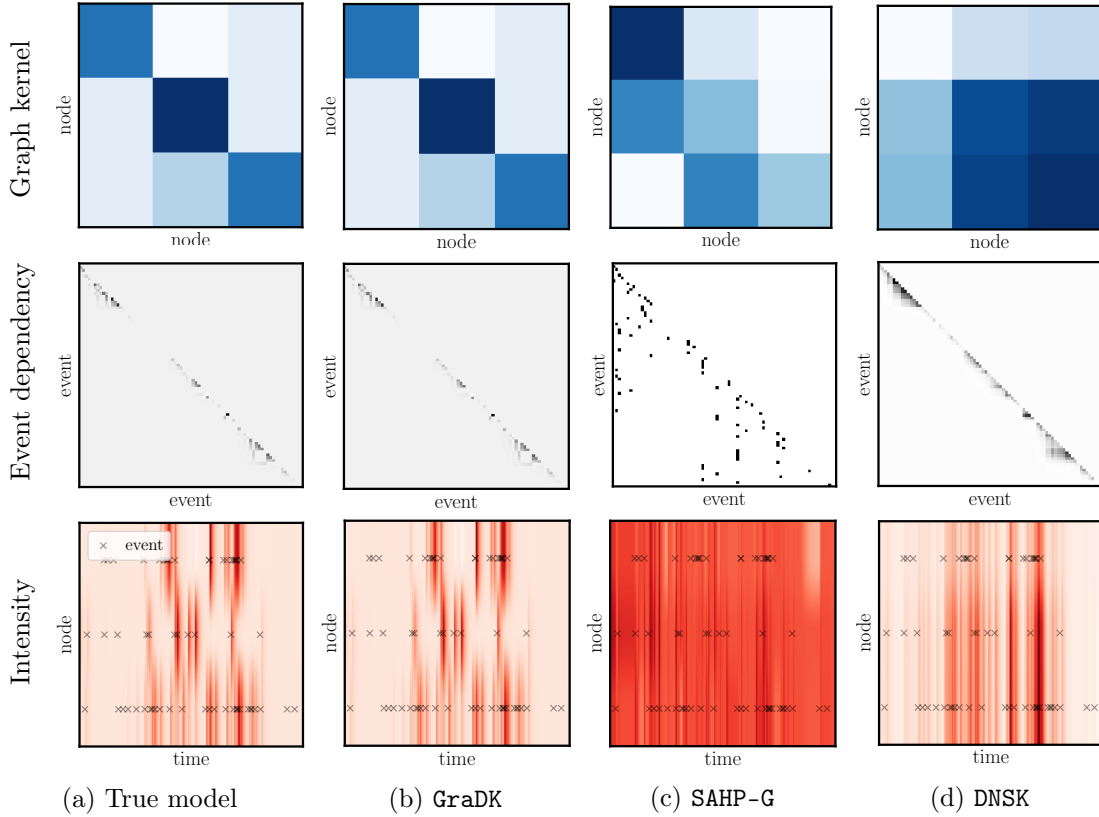


Figure A.3: Graph kernel, inter-event dependence, and conditional intensity recovery for the 3-node-graph synthetic data set with negative (inhibitive) graph influence.

patterns by taking advantage of the graph structure and GNNs. While the attention structures adopted in SAHP contribute to improved model prediction performance for future events, this approach suffers from the limited model expressiveness and interpretability when attempting to recover the underlying mechanism of the event generation process, indicated by the weak and noisy graph signals. DNSK fails to uncover the intricate patterns existing in graph kernels and only provides restrictive kernels for event modeling without considering the latent graph structures among data.

Our model not only achieves exceptional interpretability but also holds practical significance in the context of real-world point process data modeling. This can be demonstrated through experimental results conducted on traffic data. The five traffic sensors from which we collect data can be categorized into two groups, northbound sites and southbound sites, according to the directions of the highway they are monitoring. Figure A.5(a) visualizes the structure of the traffic network with sensors (graph nodes) labeled and arrows indicating the highway directions. We then investigate the conditional intensity learned by GraDK on each traffic sensor. Figure A.5(b)(c) show the conditional intensity functions of five sensors during one single day (*i.e.*, computed given one sequence from the testing set) with two subgroups of northbound and southbound sites. Note that similar temporal patterns can be found within the same subgroup, which can be attributed to the

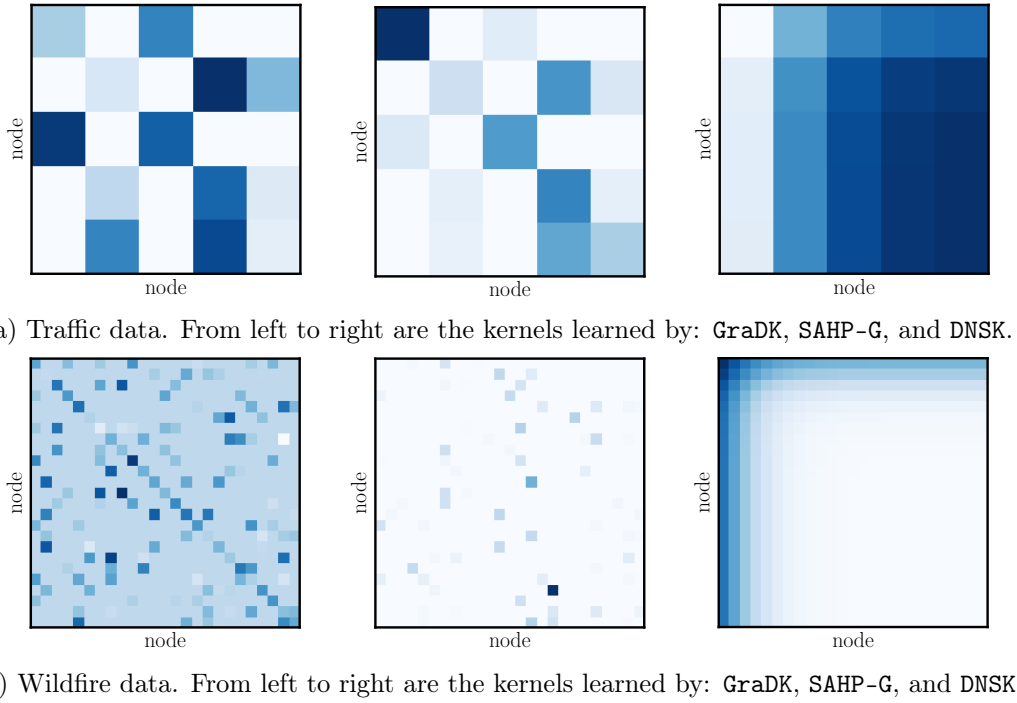


Figure A.4: Learned graph kernels for traffic and wildfire data set. The columns present the recovered kernels on each data set of **GraDK**, **SAHP-G**, and **DNSK**, respectively.

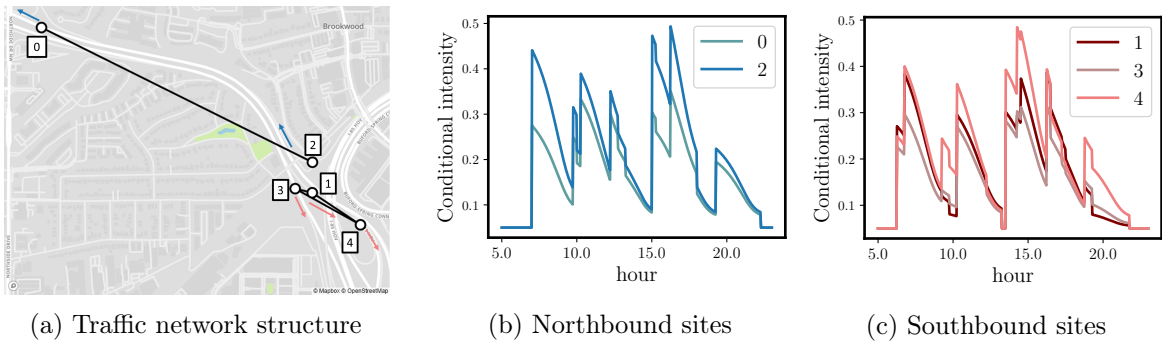


Figure A.5: (a) Traffic network structure. Each traffic sensor is labeled with a number. The blue and pink arrows indicate the monitored traffic directions of sensors on northbound and southbound highways, respectively. (b)(c) Conditional intensity of five sensors in a single day, which are categorized into two groups according to the monitored traffic directions of the sensors.

fact that the sensors in the same group are in the same direction and share the same traffic flow. Also, all the intensity functions show a temporal pattern in which they reach pinnacles during the morning (around 8:00) and evening (around 17:00) rush hours, with a higher possibility for traffic congestion at southbound sensors in the afternoon.